

# Atomic force microscopy's path to atomic resolution

Franz J. Giessibl

We review the progress in the spatial resolution of atomic force microscopy (AFM) in vacuum. After an introduction of the basic principle and a conceptual comparison to scanning tunneling microscopy, the main challenges of AFM and the solutions that have evolved in the first twenty years of its existence are outlined. Some crucial steps along the AFM's path towards higher resolution are discussed, followed by an outlook on current and future applications.

*Review Feature, submitted to Materials Today Feb 10 2005, 2nd revised version*

Experimentalphysik VI, EKM,  
Institute of Physics, Augsburg University,  
86135 Augsburg, Germany,  
Email: franz.giessibl@physik.uni-augsburg.de

**Atomic force microscopy, invented<sup>1</sup> and also introduced<sup>2</sup> in 1985/86, can be viewed as a mechanical profiling technique that generates three-dimensional maps of surfaces by scanning a sharp probe attached to a cantilever over a surface. The forces that act between the tip of the cantilever and the sample are used to control the vertical distance. AFM's potential to reach atomic resolution was foreseen in the original scientific publication,<sup>2</sup> but for a long time, the spatial resolution of AFM was inferior to the resolution capability of its parent, scanning tunneling microscopy (STM). The resolution limits of STM and AFM are given by the structural properties of the atomic wavefunctions of the probe tip and the sample. STM is sensitive to the most loosely bonded electrons with an energy at the Fermi level while AFM responds to all electrons, including core electrons. Because the**

electrons at the Fermi level are spatially less confined than core electrons that contribute to AFM images, in theory AFM should be able to achieve even greater spatial resolution than STM. Today, experimental evidence emerges where in simultaneous AFM/STM studies, AFM images reveal even finer structural details than simultaneously recorded STM images. The experimental advances that made high-resolution AFM possible started with the introduction of frequency modulation AFM (FM-AFM), where the cantilever oscillates at a fixed amplitude and the frequency is used as a feedback signal. Early implementations of FM-AFM utilized silicon cantilevers with a typical spring constant of 10 N/m that oscillate with an amplitude on the order of 10 nanometers. The spatial resolution could be increased by the introduction of quartz cantilevers with a stiffness on the order of 1 kN/m, allowing the use of sub-nm amplitudes. The direct evaluation of higher harmonics in the cantilever motion has enabled a further increase in spatial resolution. Because AFM can image insulators as well as conductors, it is now a powerful complement to STM for atomically resolved surface studies. Immediate applications of high resolution AFM have been demonstrated in vacuum studies relating to materials science, surface physics and -chemistry. Some of the techniques developed for ultrahigh-vacuum AFM may be applicable to increase AFM resolution in ambient or liquid environments, such as required for studying biological or technological specimens.

## 1 Introduction

In terms of the operating principle, atomic force microscopy (AFM)<sup>1,2</sup> can be viewed as an extension of the toddlers way of ‘grasping’ the world by touching and feeling as indicated in Figure 1 of Binnig and Rohrer’s article ‘*In touch with atoms*’,<sup>3</sup> where a finger profiles an atomic surface. Likewise, one could argue that stylus profilometry is a predecessor of AFM. However, AFM and stylus profilometry have as much in common as a candle and a laser. Both of the

latter generate light, and even though candles are masterpieces of engineering,<sup>4</sup> the laser is a much more advanced technological device requiring a detailed knowledge of modern quantum mechanics.<sup>5</sup> While stylus profilometry is an extension of human capabilities that have been known for ages and works by classical mechanics, AFM requires a detailed understanding of the physics of chemical bonding forces and the technological prowess to measure forces that are several orders of magnitude smaller than the forces acting in profilometry. Only the spectacular spatial resolution of scanning tunneling microscopy (STM) could trigger the hope that the force acting between any STM tip and sample might lead to atomic force microscopy capable of true atomic resolution. The STM, established in 1981, is the first instrument that has allowed to image surfaces with atomic resolution in real space.<sup>6,7</sup> The atomic imaging of the  $7\times 7$  reconstruction of Si (111) by STM in 1983<sup>8</sup> has later helped to solve one of the most intriguing problems of surface science at that time and establish the dimer-adatom-stacking fault model by Takayanagi et al.<sup>9</sup> The capability of atomic resolution by STM provided immediate evidence for the enormous value of this instrument as a tool for surface scientists. STM can only be used on conductive surfaces. Given that many surfaces of technological interest are conducting or at least semiconducting, this may not seem to be a severe shortcoming. One might think that an STM should be capable of mapping the surface of a metallic surface at ambient conditions. However, this is not feasible, because the pervasive layer of oxides and other contaminants occurring at ambient conditions prevents stable tunneling conditions. Electrical conductivity is a necessary, but not a sufficient condition for a surface to be imaged by STM with atomic resolution, because surfaces need to be extremely clean on an atomic level. Except for a few extremely inert surfaces such as graphite, atomic resolution is only possible in an ultra-high vacuum with a pressure on the order of  $10^{-8}$  Pa and special surface preparation. The invention of the AFM by Binnig<sup>1</sup> and its introduction by Binnig, Quate and Gerber<sup>2</sup> opened the possibility of obtaining true atomic resolution on conductors *and* insulators. Indeed, it took only a short

time after the AFM's invention before apparently atomic resolution on conductors<sup>10</sup> and insulators<sup>11-13</sup> was obtained. While these early results reproduced the periodic lattice spacings of the samples that were studied, single defects or step edges were not observed. Also, the forces that acted between tip and sample were often orders of magnitudes larger than the forces that a tip with a single front atom was expected to be able to sustain. Therefore, it was commonly assumed that *many* tip atoms interacted with the surface at the same time in these early experiments. The difference between *apparent* and *true* atomic resolution of a tip with many atomic contacts can be illustrated by a macroscopic example: When profiling an egg crate with a single egg, its trajectory would represent the overall periodicity of the crate as well as a dented hump or a hole. However, when profiling one egg crate with another egg crate, again its periodicity would be retained, but holes or dented humps would pass undetected. A similar effect can occur when an AFM tip probes a surface. As long as single defects, steps or other singularities are not observed, a clear proof for *true* atomic resolution is not established. Even though atomic resolution was hardly ever achieved in initial AFM experiments, the technique was readily accepted and found many technological and scientific applications. The installed base of atomic force microscopes rapidly outnumbered their STM counterparts. A recent survey<sup>14</sup> about the ten most highly cited publications of *Physical Review Letters* ranks the original AFM publication<sup>2</sup> as number four (4251 citations as of Mar 11 2005 [ISI]) – in good company with other breakthroughs in theoretical and experimental physics that have shaped our scientific life. Most of these citations refer to AFM where the spatial resolution is ‘only’ in the nanometer-range, but the large number proves the vast applications of AFM. In spite of the rapid growth of AFM applications, matching and even exceeding the spatial resolution of STM, its parent, had to wait for new experimental developments.

## 2 Challenges of atomic resolution AFM

The technological foundations for the feasibility of STM with atomic resolution (theory of electron tunneling, mechanical actuation with pico-meter precision, vacuum technology, surface- and tip preparation, vibration isolation, ...) were probably available a few decades before 1981, but it took the bold approach by Gerd Binnig, Heinrich Rohrer, Christoph Gerber and Edi Weibel to pursue atomic resolution in real space. Binnig and Rohrer were rewarded with the Nobel Prize in Physics in 1986 (together with Ernst Ruska, the inventor of Electron Microscopy) and the AFM principle was published in the same year. The challenges of AFM with true atomic resolution are even more daunting than the hurdles that troubled STM. To start our discussion of the special AFM challenges, we first look at the physics behind STM. Figure 1 (a) shows a schematic view of a sharp tip for STM or AFM close to a crystalline sample and Fig. 1 (b) is a plot of the tunneling current and forces between tip and sample. When tip and sample are conductive and a bias voltage is applied between them, a tunneling current can flow. The red curve in Fig. 1 (b) shows the distance dependence of the tunneling current  $I_t$ . The exponential decay of  $I_t$  with distance at a rate of approximately one order of magnitude per 100 pm distance increase is the key physical characteristic that makes atomic resolution STM possible. Because of its strong decay rate, the tunneling current is spatially confined to the front atom of the tip and flows mainly to the sample atom next to it (indicated by red circles in Fig. 1 (a)). A second helpful property of the tunneling current is its monotonic distance dependence. It is easy to build a feedback mechanism that keeps the tip at a constant distance: if the actual tunneling current is larger than the setpoint, the feedback needs to withdraw the tip and vice versa. The tip sample force  $F_{ts}$ , in contrast, does not share the helpful key characteristics of the tunneling current. First,  $F_{ts}$  is composed of long-range background forces depicted in light-blue in Fig. 1 (b) and originating from the atoms colored light-blue in Fig. 1 (a) and a short-range component

depicted in blue in Fig. 1 (b) and confined to the atoms printed in blue in Fig. 1 (a). Because the short-range force is not monotonic, it is difficult to design a feedback loop that controls distance by utilizing the force. A central task to perfect AFM is therefore the isolation the front atom's force contribution and the creation of a linear feedback signal from it.

Even if it was possible to isolate the short-range force, a more basic problem needs to be solved first: how to measure small forces. For example, commonly known force meters such as precise scales are delicate and expensive instruments and even top models rarely exceed a mass resolution of  $100\text{ }\mu\text{g}$ , corresponding to a force resolution of  $1\text{ }\mu\text{N}$ . In addition, high-precision scales take about one second to acquire a weight measurement so the bandwidth is only 1 Hz. The force meters in AFM, in contrast, require a force resolution of at least a nano-Newton at a typical bandwidth of 1 kHz. Most force meters determine the deflection  $q'$  of a spring with given spring constant  $k$  that is subject to a force  $F$  with  $F = q'/k$ . Measuring small spring deflections is subject to thermal drift and other noise factors, resulting in a finite deflection measurement accuracy  $\delta q'$ . The force resolution is thus given by  $\delta F = \delta q'/k$ , and soft cantilevers provide less noise in the force measurement. In contact-mode AFM, where the tip feels small repulsive forces from the sample surface, the cantilever should be softer than the bonds between surface atoms (estimated at  $\approx 10\text{ N/m}$ ), otherwise the sample deforms more than the cantilever.<sup>15</sup> Because of noise and stability considerations, spring constants below 1 N/m or so have been chosen for AFM in contact mode. However, atomic forces are usually attractive in the distance regime that is best suited for atomic resolution imaging (approximately a few hundred pm before making contact), and soft cantilevers suffer from a "jump-to-contact" phenomenon, i.e. when approaching the surface, the cantilever snaps towards the surface ended by an uncontrolled landing. While true atomic resolution by contact-mode AFM has been demonstrated on samples that are chemically inert,<sup>16,17</sup> this method is not feasible for imaging reactive surfaces where strong attractive short-range forces act. The long-range attractive forces

have been compensated in these experiments by pulling at the cantilever (negative loading force) after jump-to-contact<sup>16</sup> or by immersing cantilever and sample in water to reduce the van-der-Waals attraction.<sup>17</sup> Howald et al.<sup>18</sup> could partially solve the reactivity problem by passivating the reactive Si tip with a thin layer of poly-tetra-fluor-ethylen (teflon). The unit cell of Si(111)-(7×7) was resolved, but atomic resolution was not reported with that method of tip passivation.

In summary, AFM shares the challenges that are already known from STM and uses many of its design features (actuators, vibration isolation etc.), but nature has posed four extra problems for atomic resolution AFM: 1. Jump-to-contact, 2. Non-monotonic short range forces, 3. Strong long-range background forces and 4. Instrumental noise in force measurements.

### 3 Frequency modulation atomic force microscopy

Dynamic AFM modes<sup>19–21</sup> help to alleviate two of the four major AFM challenges. Jump-to-contact can be prevented by oscillating the cantilever at a large enough amplitude  $A$  such that the withdrawing force on the cantilever given by  $k \times A$  is larger than the maximal attractive force.<sup>22</sup> Because the noise in cantilever deflection measurements has a component that varies in intensity inversely with frequency ( $1/f$ -noise), dynamic AFM modes are less subject to noise than quasistatic operating modes. Non-monotonic interactions and strong long-range contributions are still present.

In amplitude modulation AFM,<sup>19</sup> the cantilever is driven at a constant frequency and the vibration amplitude is a measure of the tip-sample interaction. In 1991, Albrecht et al. have shown that frequency modulation (FM) AFM<sup>20</sup> offers even less noise at larger bandwidth than amplitude modulation AFM. In FM-AFM, a cantilever with a high quality factor  $Q$  is driven to oscillate at its eigenfrequency by positive feedback with an electronic circuit that keeps the amplitude  $A$  constant. A cantilever with a stiffness of  $k$  and effective mass  $m$  has an eigenfrequency given by  $f_0 = 1/(2\pi)\sqrt{k/m}$ . When the cantilever is exposed to a tip-sample force

gradient  $k_{ts}$ , its frequency changes instantly to  $f = f_0 + \Delta f = 1/(2\pi)\sqrt{k'/m}$  with  $k' = k + k_{ts}$  (see Fig. 2). When  $k_{ts}$  is small compared to  $k$ , the square root can be expanded and the frequency shift is simply given by<sup>20</sup>

$$\Delta f(z) = \frac{f_0}{2k} k_{ts}(z). \quad (1)$$

This formula is only correct if  $k_{ts}$  is constant over the distance range from  $z - A$  to  $z + A$  that is covered by the oscillating cantilever. The force gradient  $k_{ts}$  was probably almost constant within the oscillation interval in the first application of FM-AFM in magnetic force microscopy by Albrecht et al.,<sup>20</sup> where magnetic recording media with magnetic transitions spaced by about  $2 \mu\text{m}$  were imaged with a cantilever with a stiffness of about  $10 \text{ N/m}$  oscillating at an amplitude of about  $5 \text{ nm}$ . In contrast, in the newer application of FM-AFM in atomic-resolution AFM, the force gradient varies by orders of magnitude throughout the oscillation of the cantilever. Using frequency modulation AFM, true atomic resolution on Si(111)-(7×7), a fairly reactive sample, could be achieved in 1994.<sup>23</sup> Figure 3 shows the topographic image of this data. The fast scanning direction was horizontal, and the atomic contrast is rather poor in the lower section, quite good in a narrow strip in the center part and vanishing in the top section. These changes in contrast were due to tip changes, indicating fairly strong interaction during the imaging process. A piezoresistive cantilever made of Si<sup>24</sup> as shown in Fig. 4(a) with a stiffness of  $17 \text{ N/m}$  was used to obtain this image. The amplitude of the cantilever can be freely adjusted by the operator, and while it was even planned to use the thermally excited amplitude<sup>25</sup> ( $\approx 10 \text{ pm}$ ), the empirically determined optimal amplitude values were always around  $10 \text{ nm}$  – on a similar order of magnitude as the value of  $A = 34 \text{ nm}$  used in the data of Fig. 3. The chemical bonding forces that are responsible for the atomic contrast in imaging Si by AFM have a range on the order of  $100 \text{ pm}$ ,<sup>26</sup> and the amplitude was 340 times as large. The requirement of such a large amplitude is in stark contrast to intuition. Imagine an atom magnified to a size of an orange

with a diameter of 8 cm. The range of the bonding force is then only 4 cm or so, and the front atom of the cantilever would approach from a distance of 20 m and only in the last few centimeters of its oscillation cycle would feel the attractive bonding forces from the sample atom next to it. On the other hand, force gradients can be quite large in chemical bonds. According to the well-known Stillinger-Weber potential,<sup>27</sup> a classic model potential the interaction of Si atoms in the solid and liquid phases, a single bond between two Si atoms has a force gradient of  $k_{ts} \approx +170 \text{ N/m}$  at the equilibrium distance of  $z = 235 \text{ pm}$  and  $k_{ts} \approx -120 \text{ N/m}$  when the two Si atoms are at a distance of  $z = 335 \text{ pm}$ . Because of the relatively large values of interatomic force gradients, even cantilevers with a stiffness on the order of 1 kN/m should be subject to significant frequency shifts when oscillating at small amplitudes (page 5 in Ref<sup>28</sup>).

Nevertheless, the large-amplitude FM technique has celebrated great successes by imaging metals, semiconductors and insulators with true atomic resolution.<sup>29–33</sup>

## 4 The search for optimal imaging parameters

In order to understand why these large oscillation amplitudes were necessary, a quantitative analysis of the physics of large amplitude FM-AFM was necessary, starting with a calculation of frequency shift for large amplitudes. If  $k_{ts}$  is not constant over one oscillation cycle, Eq. 1 no longer holds and perturbation theory such as the Hamilton-Jacobi theory<sup>34</sup> can be used to find the relationship between frequency and tip sample forces.<sup>22</sup> Other perturbative approaches have confirmed the result,<sup>35–38</sup> and an instructive representation of the formula is

$$\Delta f(z) = \frac{f_0}{\pi k} \int_{-1}^1 k_{ts}(z - uA) \sqrt{1 - u^2} du. \quad (2)$$

This equation is key to a physical understanding of FM-AFM allowing to evaluate the impact of various force components on  $\Delta f$ , the experimental observable. On a first glance, the large-amplitude result resembles Eq. 1 where  $k_{ts}(z)$  is replaced by an averaged value. The average

force gradient is computed by convoluting  $k_{ts}(z)$  in the interval  $z - A$  to  $z + A$  with a semi-spherical weight function. The weight function has its maximum at  $u = 0$  – a distance  $A$  away from the minimal tip-sample distance. The minimal tip sample distance  $z_{min}$  is an important parameter in any STM or AFM experiment, because while a small value of  $z_{min}$  is desirable for optimal spatial resolution, both tip and sample can be damaged if  $z_{min}$  is too small. We can now ask, if we keep  $z_{min}$  constant and vary  $A$ , what happens to our signal, the frequency shift  $\Delta f$ ? The answer is given in Eq. 2: as long as the gradient of the tip-sample interaction  $k_{ts}$  remains constant as the tip of the cantilever moves over a  $z$ -range from  $z_{min}$  to  $z_{min} + 2A$ ,  $\Delta f$  stays constant. However, as  $A$  reaches the decay length  $\lambda$  of the interaction, the frequency shift drops sharply at a rate  $\propto (\lambda/A)^{3/2}$ . It turns out that for amplitudes larger than  $\lambda$ ,  $\Delta f$  is no longer proportional to the force gradient, but to the product of force and the square root of  $\lambda$ <sup>39</sup> (or, equivalently to the geometric average between potential and force<sup>40</sup>). In FM-AFM with amplitudes large compared to the interaction range, it is useful to define a quantity  $\gamma = \Delta f k A^{3/2} / f_0$ .<sup>22</sup> The 'normalized frequency shift'  $\gamma$  connects the physical observable  $\Delta f$  and the underlying forces  $F_{ts}$  with range  $\lambda$ , where  $\gamma \approx 0.4 F_{ts} \lambda^{1/2}$  (see Eqs. 35-41 in<sup>33</sup>). For covalent bonds, the typical bonding strength is on the order of -1 nN with  $\lambda \approx 1 \text{ \AA}$ , resulting in  $\gamma \approx -4 \text{ fN} \sqrt{\text{m}}$ , where a negative sign indicates attractive interaction. The crossover from the small-amplitude approximation in Eq. 1 to the large-amplitude case in Eq. 2 occurs for amplitudes on the order of the interaction range  $\lambda$ .

Equation 2 determines the influence of the oscillation amplitude on AFM challenge number 3 (disturbing contribution of long-range forces) outlined in the second section: Imagine an AFM tip at a minimal distance  $z_{min} = 0.3 \text{ nm}$  to a surface, where the total tip-sample force is composed of a chemical bonding force with an exponential distance dependence and a given range with a long-range force with the same strength and a ten times longer range (see caption of Table 1 for details). In large-amplitude AFM (here,  $A > 1 \text{ nm}$ ), the signal is proportional to

the normalized frequency shift  $\gamma$ , and the long-range contribution to  $\Delta f$  is  $\sqrt{1 \text{ nm}/100 \text{ pm}} \approx 3$ -times larger than the short-range contribution. For small amplitudes (here,  $A < 100 \text{ pm}$ ),  $\Delta f$  is proportional to the force gradient and the long-range component is only  $100 \text{ pm}/1 \text{ nm} = 1/10$  of the short-range contribution. Therefore, small amplitude AFM helps to reduce the unwanted contribution of long-range forces.

Even stronger attenuation of the unwanted long-range contribution would be possible if higher order force derivatives could be mapped directly. For example, if we could directly measure  $\partial^2 F_{ts}/\partial z^2$ , the long range component was only 1/100 of the short-range contribution, and for a direct mapping of the third order gradient  $\partial^3 F_{ts}/\partial z^3$ , the relative long range component would reduce to a mere 1/1000. Higher force gradients can be mapped directly by higher-harmonic AFM, as shown further below.

AFM method	physical observable	short-range contribution	long-range contribution	relative short-range contribution
quasistatic	force	1 nN	1 nN	50 %
large amplitude FM	$\gamma \approx 0.4 \times \text{force} \times \sqrt{\text{range}}$	$4 \text{ fN} \sqrt{\text{m}}$	$12 \text{ fN} \sqrt{\text{m}}$	25 %
small amplitude FM	force gradient	10 N/m	1 N/m	91 %
higher-harmonic	$n$ -th force gradient	$10^{n+9(n-1)} \text{ N/m}^n$	$10^{9(n-1)} \text{ N/m}^n$	$\approx 100 \%(1 - 10^{-n})$

Table 1: Short- and long-range contributions to AFM signals in different operating modes. This model calculation assumes a chemical bonding force  $F(z) = F_0 e^{-z/\lambda}$  with a strength of  $F_{\text{short range}}(z_{\min}) = 1 \text{ nN}$  and a range of  $\lambda_{\text{short range}} = 100 \text{ pm}$  and an equally strong long-range background force with  $F_{\text{long range}}(z_{\min}) = 1 \text{ nN}$  and a range of  $\lambda_{\text{long range}} = 1 \text{ nm}$ . Depending on the mode of AFM operation, the short-range part has a different weight in the total interaction signal. Higher-harmonic AFM offers the greatest attenuation of long-range forces.

Because the forces that act in AFM are small, optimizing the signal-to-noise ratio is crucial for obtaining good images. Frequency noise in FM-AFM is inversely proportional to amplitude.<sup>19, 20, 33, 41</sup> As discussed above, the signal stays constant until  $A$  reaches  $\lambda$  and drops proportional to  $(\lambda/A)^{3/2}$  for larger amplitudes. Therefore, the signal-to-noise ratio is maximal for amplitudes on the order of the decay length of the interaction that is used for imaging.<sup>42</sup> For

atomic imaging, amplitudes on the order of 100 pm are expected to be optimal.

As a conclusion of these calculations, we find that the use of small amplitudes  $A \approx \lambda$  would have two advantages:

1. Increased signal-to-noise ratio<sup>42</sup>
2. Greater sensitivity to short-range forces.<sup>33</sup>

So why was it not feasible to use small amplitudes in the initial experiments? Two reasons, related to the mechanical stability of the oscillating cantilever, can be identified. First, jump-to-contact is prevented if the withdrawing force of the cantilever when it is closest to the sample given by  $k \times A$  is larger than the maximal attraction.<sup>22</sup> Second, because tip-sample forces are not conservative,<sup>43</sup> random dissipative phenomena with a magnitude of  $\delta E_{ts}$  cause amplitude fluctuations  $\delta A = \delta E_{ts}/(kA)$ .<sup>42,44</sup> Both problems can be resolved by utilizing cantilevers with sufficient stiffness. Stability considerations propose a lower threshold for  $k$  that depends on the tip-sample dissipation as well as the  $Q$ -factor of the cantilever. Because the frequency shift is inversely proportional to the stiffness (Eqs. 1 and 2),  $k$  should still be chosen as low as permitted by the stability requirements. Stiff cantilevers were not commercially available when we realized their potential advantages, therefore we built cantilevers with a stiffness of  $k = 1800 \text{ N/m}$  from quartz tuning forks<sup>45,46</sup> (see Fig. 4(b)). A secondary advantage of quartz cantilevers is their greater frequency stability with temperature, which leads to lower frequency drift in particular if a quartz stabilized frequency detector is used (we used the EasyPLL by Nanosurf AG, Liestal, Switzerland). Other small-amplitude approaches with stiff home-built tungsten cantilevers have been demonstrated in Ragnar Erlandsson's<sup>47</sup> and John Pethica's groups.<sup>48-50</sup> As predicted by theoretical considerations, the stiff cantilever allowed to use sub-nm amplitudes, resulting in an improved signal-to-noise ratio, a strong attenuation of the disturbing long-range forces and the possibility of stable scanning at very small tip-sample distances. For these rea-

sons, the spatial resolution was increased as shown in Fig. 5. The image shows a very clear picture of Si with a defect and very large corrugation. The adatoms of Si which should be spherically symmetric showed subatomic details that are interpreted as orbitals in the tip atom.<sup>51,52</sup> This AFM image seemed to show greater resolution than what was known from STM. According to the ‘Stoll-formula’,<sup>53</sup> a theoretical estimate of the vertical corrugation and thus the lateral resolution of STM images, two physical parameters are crucial for the high spatial resolution of STM: a) the very short decay length of the tunneling current and b) a small tip-sample distance. Three likely reasons have been identified that may explain why dynamic AFM could provide better resolution than STM:<sup>54</sup>

1. In dynamic AFM, the minimal tip sample distance can be much smaller than in STM without destroying the tip, because the shear forces that act on the front atom during scanning are much smaller in the oscillation phase where the tip is far from the sample.
2. When using large gap voltages, a variety of states can contribute to the tunneling current, smearing out the image.
3. Tip-sample forces also have repulsive components with a very short decay length.

The first two characteristics can be fulfilled in STM as well by using a very small tunneling bias voltage and oscillating the STM tip similar to an AFM tip. Figure 6 shows an image obtained in dynamic STM where a  $\text{Co}_6\text{Fe}_3\text{Sm}$  magnetic tip was mounted onto a qPlus sensor, imaging Si.<sup>55,56</sup> Each Si adatom looks like a fried egg with a sharp center peak surrounded by a halo. The radius of the center peak is only on the order of 100 pm, showing that higher-momentum states<sup>57</sup> must have been involved in this image. The experiment was repeated with pure Co, Fe and Sm tips, and only pure Sm tips yielded similar images as Figure 6, we therefore concluded that a Sm atom acted as the tip atom in this experiment.<sup>55</sup> In atomic samarium, the electrons at highest occupied state are in a 4f state. If one assumes, that the electronic states at a Sm surface

atom of bulk  $\text{Co}_6\text{Fe}_3\text{Sm}$  are similar to atomic states in Sm, it appears likely that the crystal field around the front atom creates a state close to  $4f_{z^3}$  symmetry that is responsible for the tunneling contrast. Interestingly, very small tip-sample distances could only be realized with oscillating tips. When the oscillation was turned off, the current setpoint had to be reduced otherwise the tip would not survive the small tunneling distances.

Operation at small oscillation amplitudes not only results in greater resolution, it also facilitates simultaneous STM and AFM imaging. A straightforward implementation of combined current- and force measurements uses the constant-height mode, where the  $z$ -position of the tip is held constant relative to the plane connecting the surface atoms. A simultaneous measurement of tunneling current and frequency shift allows to compare forces and tunneling currents. Figure 7 shows a comparison of current and repulsive force on graphite<sup>58</sup> observed by simultaneous AFM and STM in vacuum at liquid helium temperatures (4.9 K). STM only sees the electrons at the Fermi level, while repulsive forces act wherever the local charge density is high (i.e. over *every* atom) for small enough distances. In graphite, only every second surface atom conducts electricity, but every surface atom exerts repulsive forces. Therefore, AFM “sees more” than STM and allows to correlate topography to local conductance. This method is promising for other materials with more than one basis atom in the elementary cell. The images have been taken with a low-temperature AFM/STM operating at 4.9 K in ultra-high vacuum.<sup>59,60</sup>

While a strong bias dependence holds both for atomic-resolution STM<sup>61</sup> as well as AFM images,<sup>60,62</sup> one pronounced difference is that the direction of the tunneling current is not accessible in STM, while the direction of the measured force is determined by the orientation of the cantilever. Usually, AFM senses forces that are normal to the surface, but it is also possible to perform lateral force microscopy<sup>63</sup> by measuring the forces acting parallel to the surface. In a quasistatic mode, lateral forces can be recorded simultaneously with normal forces. In dynamic modes, it is easier to rotate the attachment of the cantilever by 90 degrees and detect lateral

forces. Figure 8 shows a measurement of the lateral force gradients between a tip and a Si surface. Parallel motion between tip and cantilever also allows to use extremely soft cantilevers without suffering jump-to-contact to probe the limits of force resolution, as demonstrated by Rugar et al. in single spin detection by magnetic resonance force microscopy.<sup>64</sup>

## 5 Higher-harmonic atomic force microscopy

Can we increase the spatial resolution of AFM any further? When decreasing the amplitude from  $A \gg \lambda$  to  $A \ll \lambda$ , the frequency shift changes from a proportionality of  $F_{ts}\sqrt{\lambda}$  to  $F_{ts}/\lambda$ . As outlined above, an experimental observable that is proportional to a higher force gradient should allow even higher spatial resolution than small-amplitude FM-AFM. Luckily, there is a physical observable that couples directly to higher force gradients. When the cantilever oscillates in the force field of the sample, a shift in frequency is not the only change in the cantilever's motions. The oscillation of the cantilever changes from a purely sinusoidal motion given by  $q' = A \cos(2\pi ft)$  to an oscillation that contains higher harmonics with  $q' = \sum_{n=0}^{\infty} a_n \cos(2\pi nft + \phi_n)$ . For amplitudes that are large with respect to the range of  $F_{ts}$ , the higher harmonics are essentially proportional to  $\Delta f$ .<sup>37</sup> However, for small amplitudes, Dürig has found that  $F_{ts}$  could be recovered immediately within the distance range from  $z_{min}$  to  $z_{min} + 2A$  if the amplitudes and phases of all higher harmonics of the cantilever's motion were known.<sup>65</sup> Moreover, higher harmonics bear even more useful information: direct coupling to higher force gradients.<sup>66</sup> Similar to Eq. 2, we can express the magnitude of the higher harmonics by a weighted average of a force gradient – a gradient of order  $n > 1$  this time:

$$a_n = \frac{2}{\pi k} \frac{1}{1 - n^2} \frac{A^n}{1 \cdot 3 \cdot \dots \cdot (2n - 1)} \int_{-1}^1 \frac{d^n F_{ts}(z + Au)}{dz^n} (1 - u^2)^{n-1/2} du. \quad (3)$$

The weight function changes from the semi-spherical shape  $w_{\Delta f}(u) = (1 - u^2)^{1/2}$  in Eq. 2 to functions  $w_n(u) = (1 - u^2)^{n-1/2}$  that are more and more peaked with increasing  $n$ . For this

reason, the use of small amplitudes is of even greater importance in higher-harmonic AFM than in FM-AFM. The magnitude of the higher harmonic amplitudes  $a_n$  is rather small compared to the fundamental amplitude  $a_1 = A$ , therefore higher harmonic AFM works best at low temperatures, where the detection bandwidth can be set to very small values.

The spatial resolution of AFM and STM is fundamentally neither limited by the mechanical vibration level nor by thermal vibrations, but by the spatial extent of the experimental objects that are observed – electrons at the Fermi level in STM,<sup>67</sup> and something close to the total charge density in repulsive AFM.<sup>68</sup> When probing the resolution limits of AFM, we first have to find an object with the desired sharply localized electronic states. Pauling<sup>69</sup> has noted, that transition metals show a covalent bonding character, and should therefore expose lobes of increased charge density towards their neighbors. Indeed, while the surface atoms of W(001) expose a large blurred charge cloud at the Fermi level for  $k$ -vectors perpendicular to the surface (Fig. 8 in Ref.<sup>70</sup>), the total charge density shows four distinct maxima (Fig. 3 in Ref.<sup>70</sup> and Fig. 3(a) in Ref.<sup>71</sup>). Figure 9 shows a direct comparison of the simultaneously recorded tunneling current and the amplitudes of the higher harmonics. As expected, the higher harmonic data shows much greater detail.

## 6 Summary and Conclusion

We have emphasized the enormous usefulness of AFM by referring to the numerous references to the original publication<sup>2</sup> in the introduction. While most AFM applications are currently not in the atomic resolution regime, the enhancement in spatial resolution is likely to add significant value in most AFM studies in physics, chemistry, biology and materials science. Recently, true atomic resolution by FM-AFM has been observed at ambient pressure in an N<sub>2</sub> atmosphere,<sup>72</sup> showing that some of the concepts of vacuum AFM are applicable in ambient environments. Although STM resolution can benefit from oscillating the tip, a concept that has originated in

AFM, Fig. 9 shows that AFM has now clearly reached and even surpassed the resolution capability of STM. Figure 10 shows the evolution of the resolution of AFM from large amplitude AFM in 1994 (a) to small amplitude AFM in 2000 (b) and higher harmonic AFM in 2004 (c). While the structures within single atoms shown in Fig. 10 (b) and (c) originate in the front atom of the probe, other examples where AFM shows more atomic details of specimens than STM such as the observation of the rest atoms in Si(111)-(7×7)<sup>73,74</sup> or the observation of all dangling bonds on the Si/Ge(105) surface<sup>75</sup> establish the improved spatial resolution of AFM over STM in special cases. Atomic- and molecular structuring has been the domain of STM for a long time, starting with the first demonstration of manipulating single atoms<sup>76</sup> to a variety of nano-structuring methods by STM.<sup>77</sup> Recently, it has been shown that atomic manipulation by AFM is possible even at room temperature.<sup>78</sup>

We have not been able to discuss the phenomenal success of AFM in biology, a field with a much more immediate impact on the human condition. It can be expected that at least some of the concepts that have been developed for AFM in vacuum will enable greater resolution in biological AFM applications as well.<sup>79,80</sup>

### **Acknowledgments**

I wish to thank Jochen Mannhart for support and editorial suggestions and my current and former students Martin Breitschaft, Philipp Feldpausch, Stefan Hembacher, Markus Herz, Christian Schiller, Ulrich Mair, Thomas Ottenthal and Martina Schmid for their contributions towards the progress of AFM. I also thank Gerd Binnig, Calvin F. Quate and Christoph Gerber for kicking off the fun of the AFM field and for ongoing inspiring interactions. Special thanks to Heinrich Rohrer, Calvin Quate and Christoph Gerber for critical comments and to German Hammerl for help with LaTeX. Supported by the Bundesministerium für Forschung und Technologie under contract 13N6918.

## References

1. Binnig, G. *Atomic Force Microscope and Method for Imaging Surfaces with Atomic Resolution* (1986) **US Patent 4,724,318**
2. Binnig, G., Quate, C. F., and Gerber, C. *Phys. Rev. Lett.* (1986) **56**, 930
3. Binnig, G. and Rohrer, H. *Rev. Mod. Phys.* (1999) **71**, S324
4. Faraday, M. *Chemical History of a Candle*. reprinted in 2003, Dover Publications, Mineola, NY (1861)
5. Siegman, A. E. *Lasers*. University Science Books, Herndon, VA, USA (1986)
6. Binnig, G., Rohrer, H., Gerber, C., and Weibel, E. *Phys. Rev. Lett.* (1982) **49**, 57
7. Hofer, W. A. *Materials Today* (2002) **October**, 24
8. Binnig, G., Rohrer, H., Gerber, C., and Weibel, E. *Phys. Rev. Lett.* (1983) **50**, 120
9. Takayanagi, K., Tanishiro, Y., Takahashi, M., and Takahashi, S. *J. Vac. Sci. Technol. A* (1985) **3**, 1502
10. Binnig, G., Gerber, C., Stoll, E., Albrecht, T. R., and Quate, C. F. *Europhys. Lett.* (1987) **3**, 1281
11. Albrecht, T. R. and Quate, C. F. *J. Appl. Phys.* (1987) **62**, 2599
12. Meyer, G. and Amer, N. M. *Appl. Phys. Lett.* (1990) **56**, 2100
13. Meyer, E., Heinzelmann, H., Rudin, H., and Güntherodt, H.-J. *Z. Phys. B* (1990) **79**, 3
14. Riordon, J. *APS News* (2003) **May issue**, 3

15. Rugar, D. and Hansma, P. *Physics Today* (1990) **43**, 23
16. Giessibl, F. J. and Binnig, G. *Ultramicroscopy* (1992) **42-44**, 281
17. Ohnesorge, F. and Binnig, G. *Science* (1993) **260**, 1451
18. Howald, L., Lüthi, R., Meyer, E., and Güntherodt, H.-J. *Phys. Rev. B* (1995) **51**, 5484
19. Martin, Y., Williams, C. C., and Wickramasinghe, H. K. *J. Appl. Phys.* (1987) **61**, 4723
20. Albrecht, T. R., Grutter, P., Horne, H. K., and Rugar, D. *J. Appl. Phys.* (1991) **69**, 668
21. Dürig, U., Züger, O., and Stalder, A. *Journal of Applied Physics* (1992) **72**, 1778
22. Giessibl, F. J. *Phys. Rev. B* (1997) **56**, 16010
23. Giessibl, F. J. *Science* (1995) **267**, 68
24. Tortonese, M., Barrett, R. C., and Quate, C. *Appl. Phys. Lett.* (1993) **62**, 834
25. Giessibl, F. J. *Jpn. J. Appl. Phys.* (1994) **33**, 3726
26. Perez, R., Stich, I., Payne, M. C., and Terakura, K. *Phys. Rev. Lett.* (1997) **78**, 678
27. Stillinger, F. H. and Weber, T. A. *Phys. Rev. B* (1985) **31**, 5262
28. Giessibl, F. J. *German Patent* (1996) Patentschrift DE 196 33 546
29. Morita, S., Wiesendanger, R., and Meyer, E., eds. *Noncontact Atomic Force Microscopy. Nanoscience and Technology*. Springer Berlin Heidelberg New York (2002)
30. Meyer, E., Hug, H. J., and Bennewitz, R. *Scanning Probe Microscopy. The Lab on a Tip*. Springer, Berlin Heidelberg New York (2003)
31. Garcia, R. and Perez, R. *Surf. Sci. Rep.* (2002) **47**, 197

32. Hofer, W. A., Foster, A. S., and Shluger, A. L. *Rev. Mod. Phys.* (2003) **75**, 1287
33. Giessibl, F. J. *Rev. Mod. Phys.* (2003) **75**, 949
34. Goldstein, H. *Classical Mechanics*. Addison Wesley, Reading MA (1980)
35. Baratoff, A. *unpublished* (1997)
36. Dürig, U. *Surf. and Interf. Anal.* (1999) **27**, 467
37. Dürig, U. *Appl. Phys. Lett.* (1999) **75**, 433
38. Livshits, A., Shluger, A., and Rohl, A. *Appl. Surf. Sci.* (1999) **140**, 327
39. Giessibl, F. J. and Bielefeldt, H. *Phys. Rev. B* (2000) **61**, 9968
40. Ke, S. H., Uda, T., and Terakura, K. *Phys. Rev. B* (1999) **59**, 13267
41. Hasegawa, Y., Eguchi, T., An, T., *et al.*. *Japanese Journal of Applied Physics* (2004) **43**, L303
42. Giessibl, F. J., Bielefeldt, H., Hembacher, S., and Mannhart, J. *Appl. Surf. Sci.* (1999) **140**, 352
43. Kantorovich, L. N. *Phys. Rev. B* (2001) **64**, 245409
44. Giessibl, F. J., Hembacher, S., Herz, M., Schiller, C., and Mannhart, J. *Nanotechnology* (2004) **15**, S79
45. Giessibl, F. J. *Appl. Phys. Lett.* (1998) **73**, 3956
46. Giessibl, F. J. *Appl. Phys. Lett.* (2000) **76**, 1470
47. Erlandsson, R., Olsson, L., and Martensson, P. *Phys. Rev. B* (1997) **54**, R8309

48. Hoffmann, P. M., Oral, A., Grimble, R. A., *et al.*. *Proc. R. Soc. London A* (2001) **457**, 1161

49. Hoffmann, P. M., Jeffery, S., Pethica, J. B., Özgür Özer, H., and Oral, A. *Physical Review Letters* (2001) **87**, 265502

50. Oral, A., Grimble, R. A., Özgür Özer, H., Hoffmann, P. M., and Pethica, J. B. *Appl. Phys. Lett.* (2001) **79**, 1915

51. Giessibl, F. J., Hembacher, S., Bielefeldt, H., and Mannhart, J. *Science* (2000) **289**, 422

52. Huang, M., Cuma, M., and Liu, F. *Phys. Rev. Lett.* (2003) **90**, 256101

53. Stoll, E. *Surf. Sci. Lett.* (1984) **143**, L411

54. Giessibl, F. J., Bielefeldt, H., Hembacher, S., and Mannhart, J. *Ann. Phys. (Leipzig)* (2001) **10**, 887

55. Herz, M., Giessibl, F. J., and Mannhart, J. *Phys. Rev. B* (2003) **68**, 045301

56. Herz, M. *Dynamische Tunnel-, Kraft- und Reibungsmikroskopie mit atomarer und subatomarer Auflösung*. Ph.D. thesis, University of Augsburg, Germany (2003)

57. Chen, C. J. *Introduction to Scanning Tunneling Microscopy*. Oxford University Press, New York (1993)

58. Hembacher, S., Giessibl, F. J., Mannhart, J., and Quate, C. F. *Proc. Natl. Acad. Sci. (USA)* (2003) **100**, 12539

59. Hembacher, S. F. *Simultane Rasterkraft- und Rastertunnelmikroskopie bei 5 K im Ultra-hochvakuum*. Ph.D. thesis, Universität Augsburg, Germany (2003)

60. Hembacher, S., Giessibl, F. J., and Mannhart, J. *Phys. Rev. Lett.* (2005) **94**, 056101

61. Feenstra, R. M., Stroscio, J. A., Tersoff, J., and Fein, A. P. *Phys. Rev. Lett.* (1987) **58**, 1192
62. Arai, T. and Tomitori, M. *Phys. Rev. Lett.* (2004) **93**, 256101
63. Mate, M., McClelland, G. M., Erlandsson, R., and Chiang, C. *Phys. Rev. Lett.* (1987) **59**, 1942
64. Rugar, D., Budakian, R., Mamin, H. J., and Chui, B. *Nature* (2004) **430**, 329
65. Dürig, U. *New Journal of Physics* (2000) **2**, 5.1
66. Hembacher, S., Giessibl, F. J., and Mannhart, J. *Science* (2004) **305**, 380
67. Tersoff, J. and Hamann, D. R. *Phys. Rev. Lett.* (1985) **50**, 1998
68. Ciraci, S., Baratoff, A., and Batra, I. P. *Phys. Rev. B* (1990) **41**, 2763
69. Pauling, L. *The Nature of the Chemical Bond*. Cornell Univ. Press, Ithaca, New York (1957)
70. Posternak, M., Krakauer, H., Freeman, A. J., and Koelling, D. D. *Phys. Rev. B* (1980) **21**, 5601
71. Mattheiss, L. F. and Hamann, D. R. *Phys. Rev. B* (1984) **29**, 5372
72. Sasahara, A., Kitamura, S., Uetsuka, H., and Onishi, H. *Journal of Physical Chemistry B* (2004) **108**, 15735
73. Lantz, M., Hug, H. J., van Schendel, P., *et al.*. *Phys. Rev. Lett.* (2000) **84**, 2642
74. Eguchi, T. and Hasegawa, Y. *Phys. Rev. Lett.* (2002) **89**, 266105
75. Eguchi, T., Fujikawa, Y., Akiyama, K., *et al.*. *Phys. Rev. Lett.* (2004) **93**, 266102

76. Eigler, D. M. and Schweizer, E. K. *Nature* (1990) **344**, 524
77. Rosei, F. *Journal of Physics-Condensed Matter* (2004) **16**, S1373
78. Sugimoto, Y., Abe, M., Hirayama, S., *et al.*. *Nature Materials* (2005) **4**, 156159
79. Miles, M. *Science* (1997) **277**, 1845
80. Horber, J. K. H. and Miles, M. J. *Science* (2003) **302**, 1002

## Figures

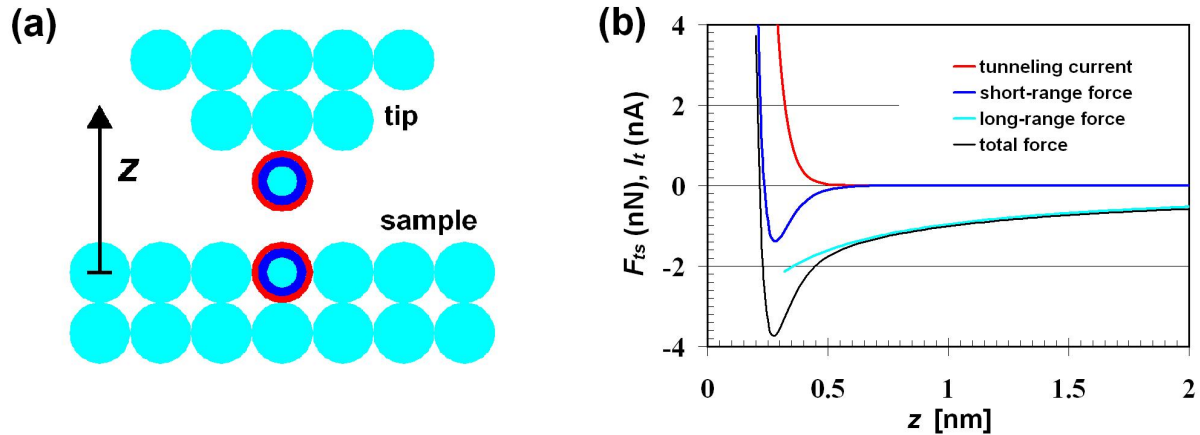


Figure 1: (a) Schematic view of a tip and a sample in a scanning tunneling microscope or atomic force microscope. The diameter of a metal atom is typically 0.3 nm. (b) Qualitative distance dependence of tunneling current, long- and short-range forces. The tunneling current increases monotonic with decreasing distance, while the force reaches a minimum and increases for distances below the bond length.

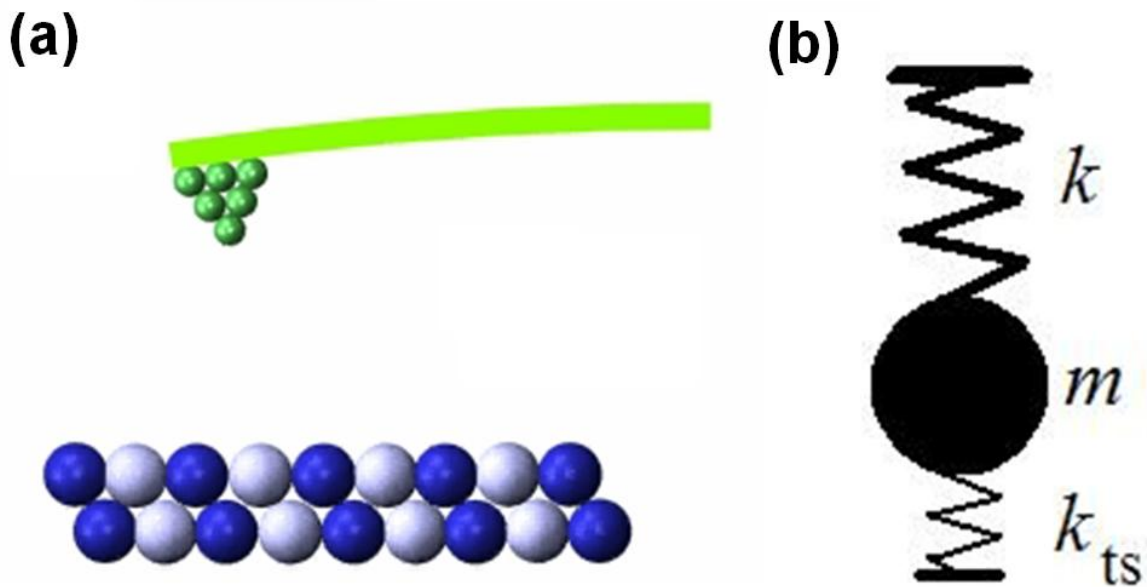


Figure 2: (a) Schematic view of a vibrating tip close to a sample in a dynamic atomic force microscope. The forces that act between the tip and the sample  $F_{ts}$  cause a detectable change in the oscillation properties of the cantilever. (b) Mechanical equivalent of (a). The free cantilever with stiffness  $k$  and effective mass  $m$  can be treated as a harmonic oscillator with an eigenfrequency  $f_0 = (k/m)^{1/2}/(2\pi)$ . The bond between tip and sample with its stiffness  $k_{ts}$  alters the resonance frequency to  $f = ([k + k_{ts}]/m)^{1/2}/(2\pi)$ . When the oscillation amplitude of the cantilever is large,  $k_{ts}$  can vary significantly within one oscillation cycle, requiring averaging (see text).

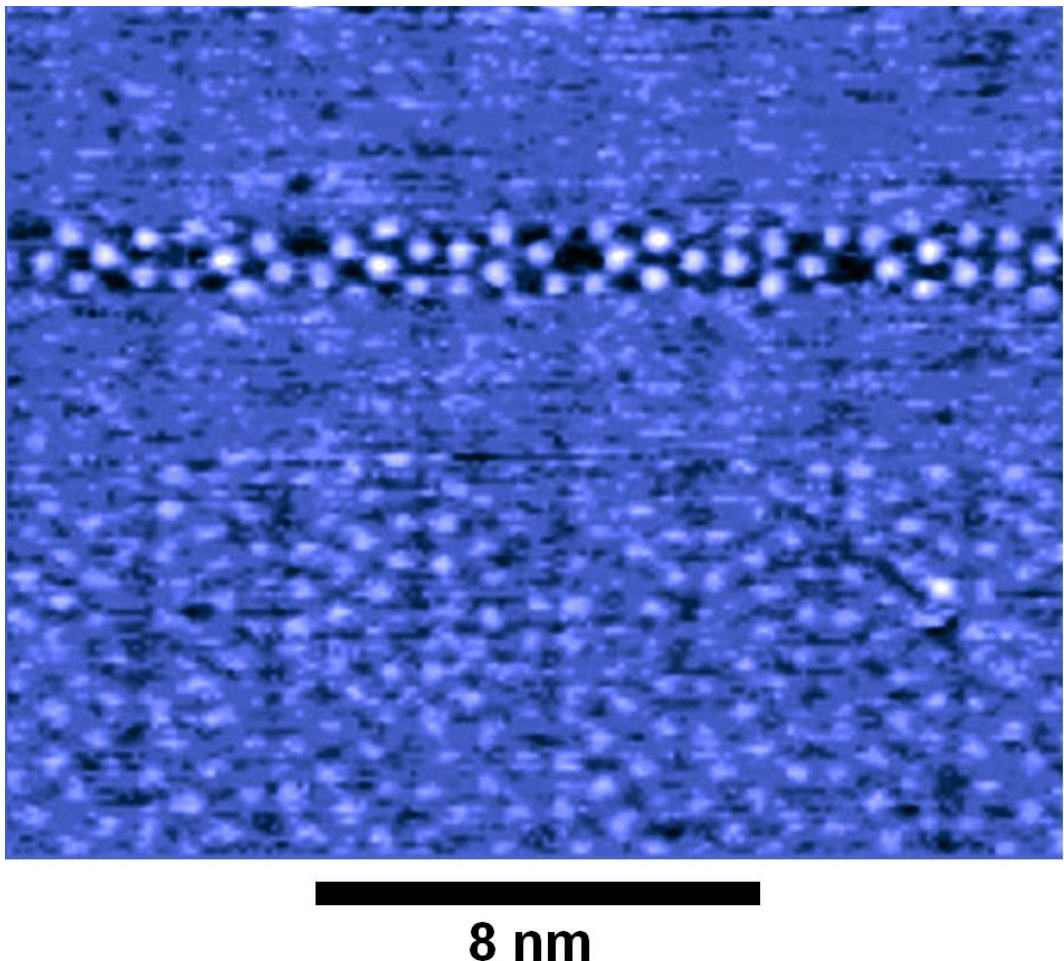


Figure 3: First AFM image of a reactive surface showing true atomic resolution: Si(111)-(7×7) reconstruction. Parameters:  $k = 17 \text{ N/m}$ ,  $A = 34 \text{ nm}$ ,  $f_0 = 114 \text{ kHz}$ ,  $\Delta f = -70 \text{ Hz}$  and  $Q = 28\,000$ , scanning speed = 3.2 lines/s. Environment: ultra-high vacuum, room temperature.<sup>23</sup>

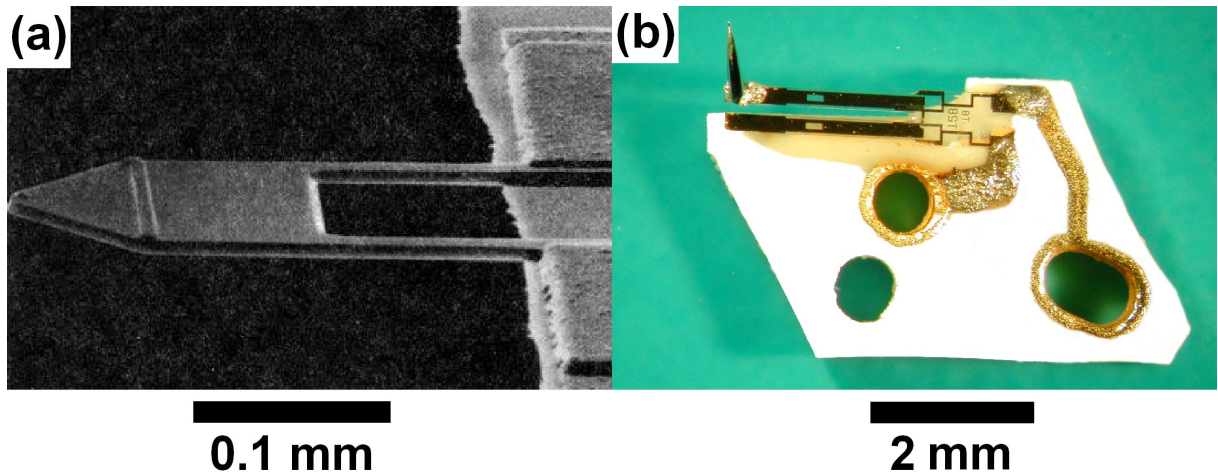


Figure 4: Micrographs of (a) a piezoresistive cantilever<sup>24</sup> and (b) a ‘qPlus’ sensor<sup>46</sup> - a cantilever made from a quartz tuning fork. The piezoresistive cantilever has a length of  $250\text{ }\mu\text{m}$ , a width of  $50\text{ }\mu\text{m}$  and a thickness of  $4\text{ }\mu\text{m}$ . The eigenfrequency is  $114\text{ kHz}$ , the stiffness  $17\text{ N/m}$  and the  $Q$ -factor in vacuum  $28\,000$ . The qPlus sensor has a typical eigenfrequency ranging from  $10$  to  $30\text{ kHz}$  (depending on the mass of the tip), a stiffness of  $1\,800\text{ N/m}$  and a  $Q$ -factor of  $4\,000$  in vacuum at  $T = 300\text{ K}$  and  $20\,000$  at  $T = 4\text{ K}$ . One of the prongs is fixed to a large substrate and a tip is mounted to the free prong. Because the fixed prong is attached to a heavy mass, the device is mechanically equivalent to a traditional cantilever. The dimensions of the free prong are: Length:  $2.4\text{ mm}$ , width:  $130\text{ }\mu\text{m}$ , thickness:  $214\text{ }\mu\text{m}$ .

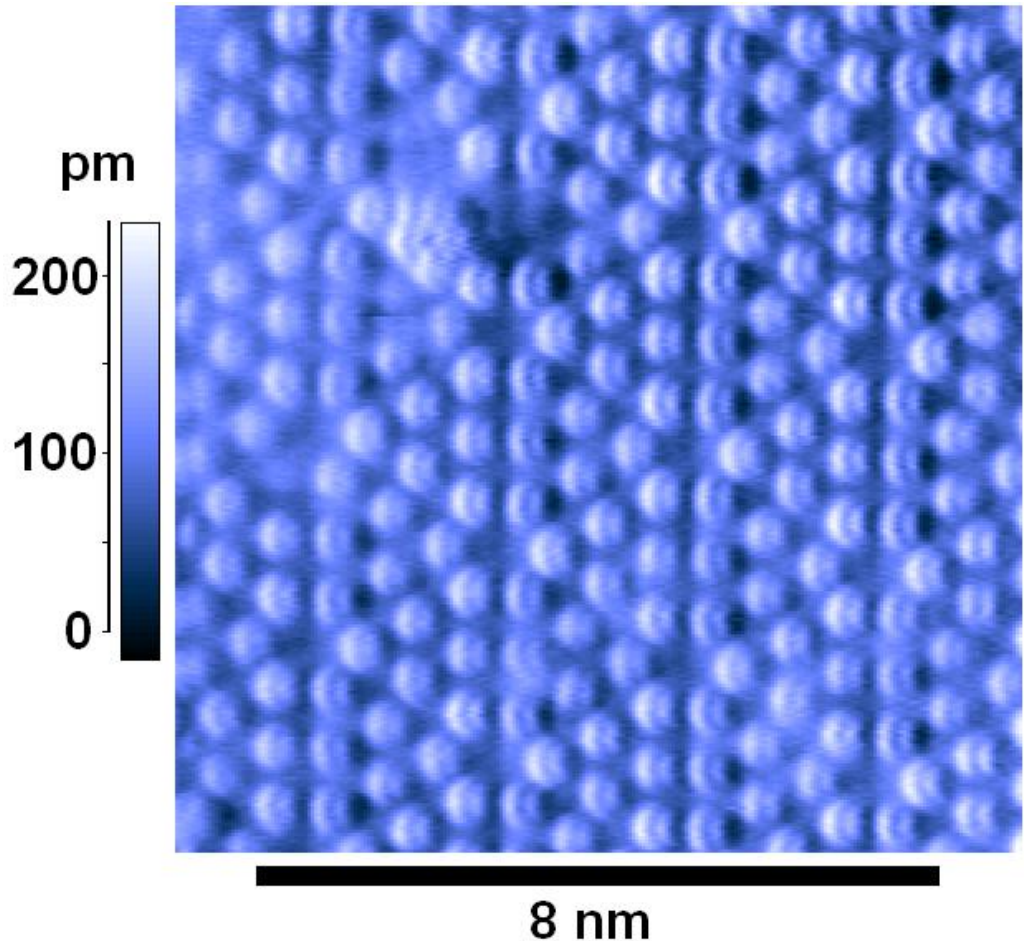


Figure 5: AFM image of the silicon  $7 \times 7$  reconstruction with true atomic resolution with a stiff cantilever. Parameters:  $k = 1800 \text{ N/m}$ ,  $A = 0.8 \text{ nm}$ ,  $f_0 = 16.86 \text{ kHz}$ ,  $\Delta f = -160 \text{ Hz}$  and  $Q = 4000$ . Environment: ultra-high vacuum, room temperature.<sup>51</sup>

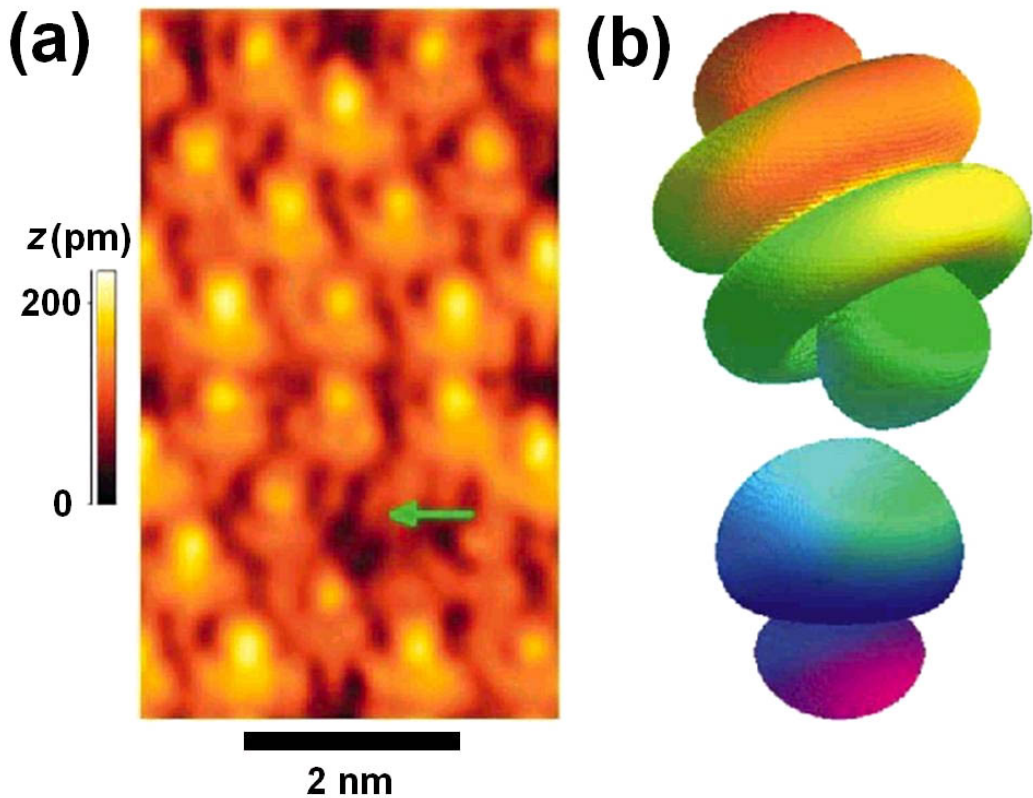


Figure 6: (a) Dynamic STM image of the silicon  $7 \times 7$  reconstruction where a  $\text{Co}_6\text{Fe}_3\text{Sm}$  tip was mounted on a qPlus sensor. Parameters:  $k = 1800 \text{ N/m}$ ,  $A = 0.5 \text{ nm}$ ,  $f_0 = 19\,621 \text{ Hz}$ , sample bias voltage  $-100 \text{ mV}$ , average tunneling current  $200 \text{ pA}$ . (b) Schematic plot of tip and sample states that can lead to the experimental image shown in (a). The sample state is a dangling bond of a Si adatom with its  $3\text{sp}^3$  symmetry, while a Sm  $4f_{z^3}$  state is taken as a tip state. Environment: ultra-high vacuum, room temperature.<sup>56</sup>

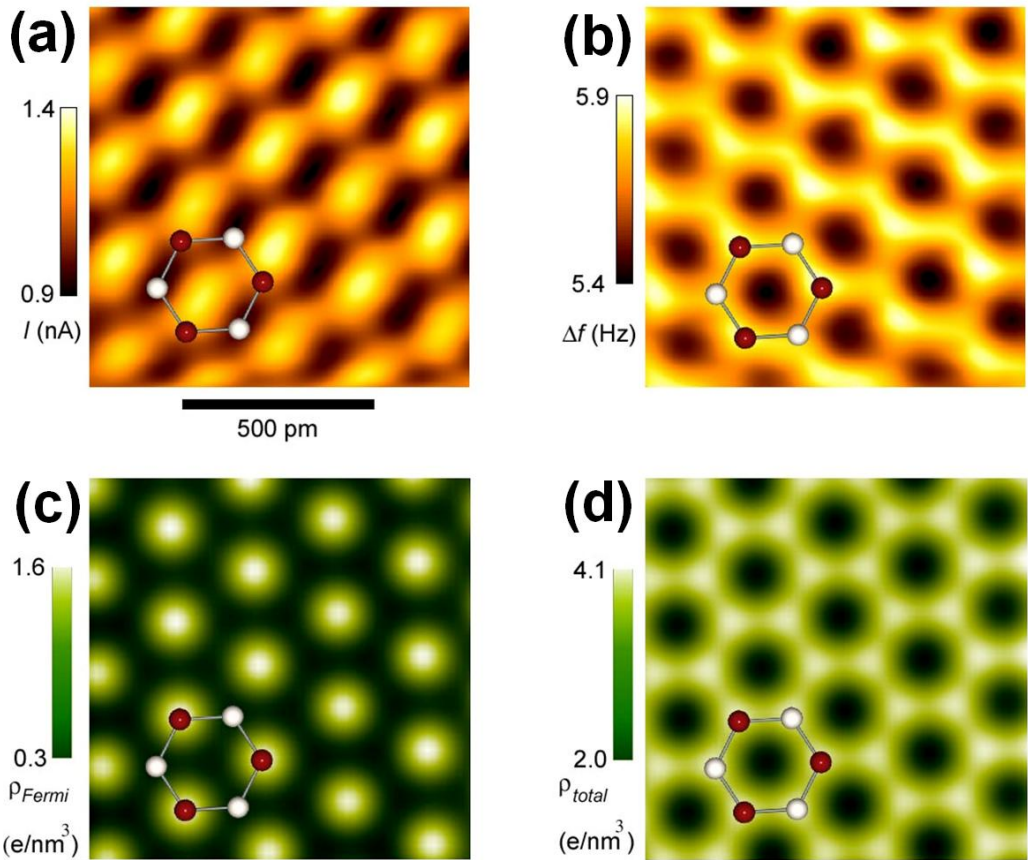


Figure 7: (a) Constant height STM image of graphite and (b) a simultaneously recorded AFM image (repulsive). Part (c) shows an estimate of the charge density at the Fermi level (visible by STM) and (d) the total charge density (relevant for repulsive AFM) for graphite. Parameters:  $k = 1800 \text{ N/m}$ ,  $A = 0.3 \text{ nm}$ ,  $f_0 = 18076.5 \text{ Hz}$ , and  $Q = 20\,000$ .<sup>58</sup>

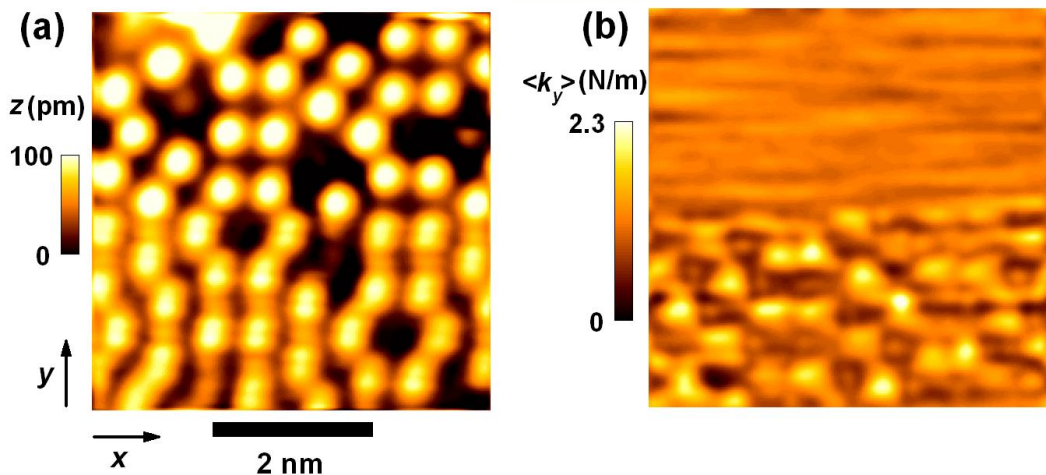


Figure 8: (a) Topographic STM image of Si(111)-(7×7) where the tip is mounted on a lateral force sensor. The tip oscillates with  $A \approx 80$  pm in the  $y$ -direction in the lower half of the image, the oscillation is turned off in the upper half. (b) Corresponding lateral force gradient. On top of the adatoms, the bond between tip and sample causes an increase in frequency shift. Parameters:  $k = 1350$  N/m,  $A = 80$  pm (bottom),  $A = 0$  (top),  $f_0 = 10214$  Hz. Environment: ultra-high vacuum, room temperature.<sup>56</sup>

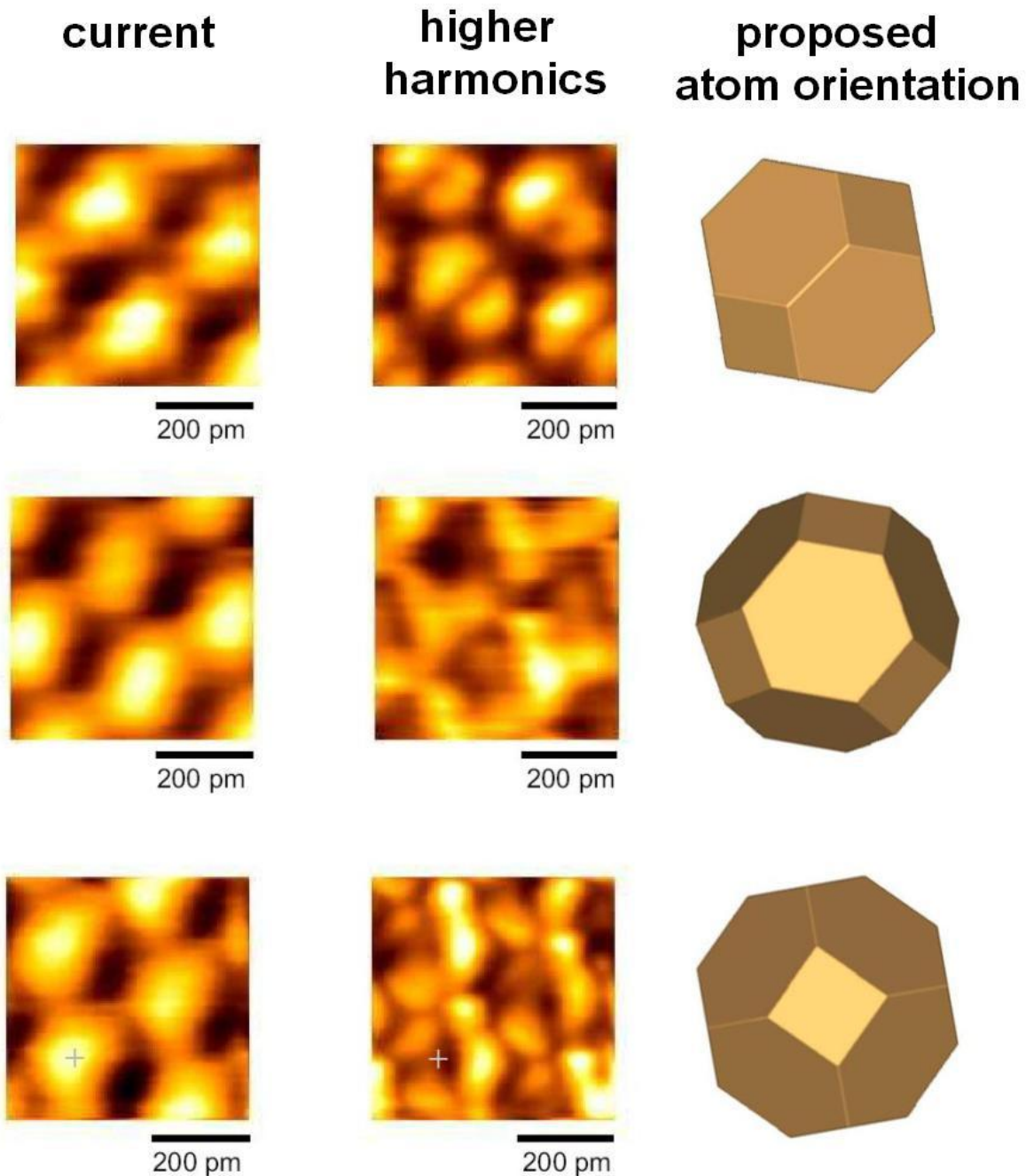


Figure 9: Simultaneous constant height STM (left column) and higher-harmonic AFM images (center column) of graphite with a tungsten tip. The right column shows the proposed orientation of the W tip atom. The W atom is represented by its Wigner-Seitz unit cell, which reflects the full symmetry of the bulk. We assume, that the bonding symmetry of the adatom is similar to the bonding symmetry of the bulk. This assumption is based on charge density calculations of surface atoms<sup>70,71</sup> In the first row, the higher harmonics show a two-fold symmetry, as resulting from a [110] orientation of the front atom. In the second row, the higher harmonics show roughly a three-fold symmetry, as expected for a [111] orientation. In the third row, the symmetry of the higher-harmonic signal is approximately four-fold, as expected for a tip in [001] orientation. Parameters:  $k = 1800 \text{ N/m}$ ,  $A = 0.3 \text{ nm}$ ,  $f_0 = 18\,076.5 \text{ Hz}$ , and  $Q = 20\,000$ . Environment: ultra-high vacuum,  $T = 4.9 \text{ K}$ .<sup>66</sup>

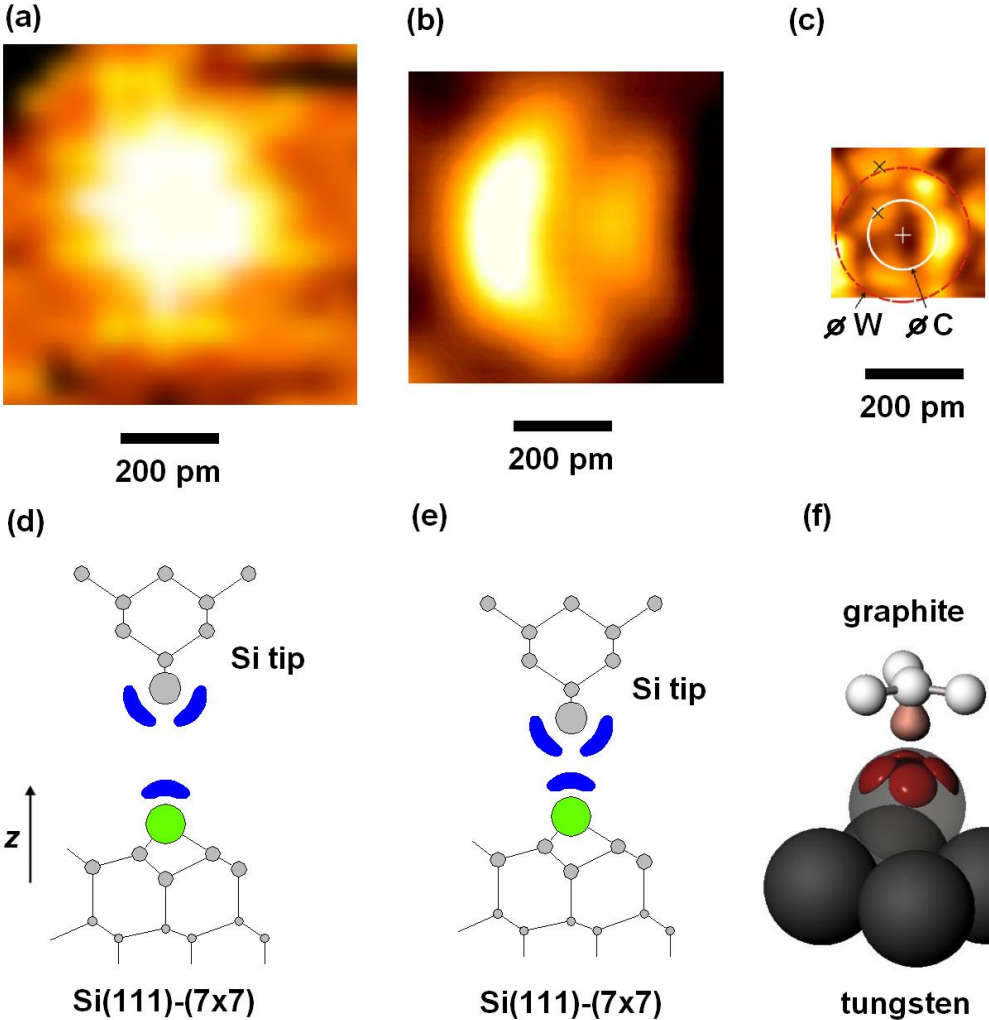


Figure 10: Progress in spatial resolution of AFM showing images of single atoms. The lateral scale in (a)-(c) is equal. (a) An adatom of the Si(111)-(7×7) reconstruction, showing up as a blurred spot. (b) An adatom of the Si(111)-(7×7) reconstruction, showing subatomic contrast originating in the electronic structure of the tip. (c) Higher-harmonic image of a tungsten atom mapped by a carbon atom. Parameters: (a)  $k = 17 \text{ N/m}$ ,  $A = 34 \text{ nm}$ ,  $f_0 = 114 \text{ kHz}$ ,  $\Delta f = -70 \text{ Hz}$  and  $Q = 28000$  (ultra-high vacuum, room temperature), (b)  $k = 1800 \text{ N/m}$ ,  $A = 0.8 \text{ nm}$ ,  $f_0 = 16860 \text{ Hz}$ ,  $\Delta f = -160 \text{ Hz}$  and  $Q = 4000$  (ultra-high vacuum, room temperature), (c)  $k = 1800 \text{ N/m}$ ,  $A = 0.3 \text{ nm}$ ,  $f_0 = 18076.5 \text{ Hz}$ , and  $Q = 20000$  (ultra-high vacuum,  $T = 4.9 \text{ K}$ ), higher harmonic detection. (d) Schematic view of a Si(001) tip close to a Si(111)-(7×7) surface. Because of the large amplitude and a fairly large minimum tip-sample distance, the blurry image (a) corresponding to this configuration is approximately symmetric with respect to the vertical axis. (e) Similar to (d), but at a closer distance. The angular dependence of the bonding forces is noticeable. (f) W(001) surface close to a C atom in a graphite surface. The charge distribution in W shows small pockets that are resolved by higher-harmonic AFM with a light-atom carbon-probe.